Optics Letters

Reduced-symmetry LMA rod-type fiber for enhanced higher-order mode delocalization

Z. Sanjabi Eznaveh,* J. E. Antonio-Lopez, J. Anderson, A. Schülzgen, and R. Amezcua-Correa

CREOL, the College of Optics and Photonics, University of Central Florida, 304 Scorpius St., Orlando, Florida 32816, USA
**Corresponding author: zahoora@knights.ucf.edu*

Received 16 February 2017; revised 10 April 2017; accepted 12 April 2017; posted 21 April 2017 (Doc. ID 286876); published 11 May 2017

We present a novel design of a micro-structured large-pitch, large-mode-area (LMA) asymmetric rod-type fiber. By reducing the cladding symmetry through six high-refractive index germanium-doped silica inclusions, the fiber features strong higher-order mode (HOM) delocalization, leading to a potentially enhanced preferential gain for the fundamental mode in active fibers. In addition, high resolution spatially and spectrally (S^2) resolved mode analysis measurements confirm HOM contributions below 1% and LP_{1m}-like HOM contributions below the detection limit. This proposed fiber design enables single-mode operation, with near-diffraction-limited beam quality of $M^2 = 1.3$ and an effective mode area of 2560 μm^2 at 1064 nm. This design opens new insights into improving the threshold-like onset of modal instabilities in high-power fiber lasers and fiber amplifiers by efficiently suppressing LP_{11} modes.

OCIS codes: (060.2280) Fiber design and fabrication; (060.4005) Microstructured fibers; (060.2430) Fibers, single-mode; (060.3510) Lasers, fiber.

https://doi.org/10.1364/OL.42.001974

Fiber lasers and fiber amplifiers have experienced considerable improvements in recent years and demonstrated remarkable power scalability [1–5]. However, due to the high optical intensity in the core, the performance of high-power fiber lasers is limited by detrimental nonlinear processes, such as four-wave mixing, self-phase modulation, stimulated Brillouin scattering, and stimulated Raman scattering. To mitigate nonlinear effects, very LMA fibers, which exhibit a mode field diameter larger than 30 μm for operation at 1064 nm have been developed [6–9]. However, such large core sizes are more prone to allow the propagation of undesired HOMs, which could potentially lead to a performance deterioration due to beam quality distortion. To suppress HOMs in LMA fibers, various advanced waveguide structures have been proposed, including large-pitch fibers (LPFs) [10,11], rod-type fibers [1,12,13], leakage channel fibers [14,15], chirally-coupled-core fibers [16,17], and fibers with resonant mode coupling of HOMs out of the core region [18,19]. Unfortunately, as the core size increases, the HOM discrimination capabilities in conventional fiber designs decrease. Consequently, LMA fibers are generally not strictly single mode, which ultimately can result in the onset of thermally induced modal instability (MI) at high average powers [4,20]. MI leads to a threshold-like degradation of the output beam quality in fiber lasers or fiber amplifiers due to the strong power coupling between the fundamental mode and HOMs [21–25]. Typically, LP_{1m}-like HOMs have the highest detrimental impact on the onset of MI because these are the modes that are most likely to be excited by a slight misalignment of the input beam [4,26]. Therefore, fibers that strongly suppress LP_{1m}-like HOMs modes are desirable to circumvent MI. In this regard, fiber designs with pentagonal, square, and heptagonal cladding microstructures have been extensively analyzed [27]. In general, these designs achieve high modal gain discrimination (i.e., the difference between the mode overlap factors of the fundamental mode and the HOMs with the doped core region), while maintaining low loss for the LP_{01} mode. In addition, it has recently been proposed that reducing the cladding symmetry of LPFs enhances the delocalization of HOMs [26,28,29]. These aperiodic LPFs enable robust and efficient single-mode operation in active fibers with mode field diameters beyond 2000 μm^2 [29].

In this Letter, we report on the design, fabrication, and detailed characterization of a passive LMA rod-type LPF with reduced cladding symmetry. The fiber incorporates six graded-index germanium-doped silica inclusions within a hexagonal lattice of air holes. The position of the high-refractive index filaments has been designed to eliminate mirror symmetries in order to reduce the overlap of the LP_{1m}-like modes with the core region. This waveguide structure improves HOM discrimination, thus allowing for robust single-mode operation and strong confinement of the LP_{01} mode within the core. Numerical simulations are in good agreement with the obtained experimental results. Moreover, S^2 mode analysis, a well-known technique for quantifying HOM content in optical fibers, reveals highly effective HOM delocalization and efficient single-mode performance.

Figure 1(a) illustrates the schematic of the reduced symmetry LMA-LPF, where white circles correspond to the air holes of diameter D, the red circles depict germanium-doped inclusions of diameter d and with a refractive index contrast $\Delta n = 30 \times 10^{-3}$, and Λ (pitch) is the distance between

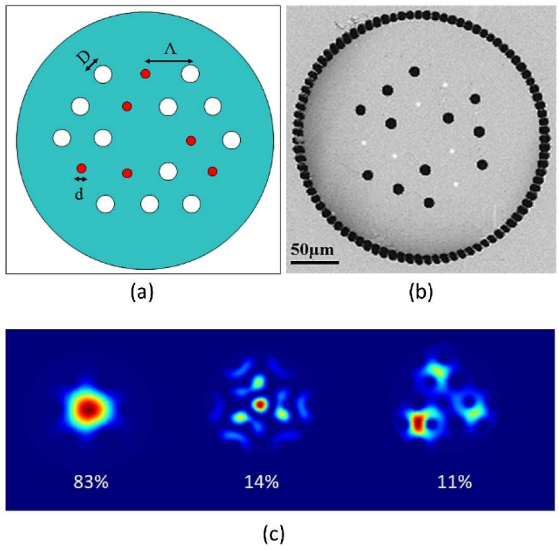

Fig. 1. (a) Schematic representation of the asymmetric LMA rod-type LPF. The white circles depict air holes of diameter D, the red circles depict germanium-doped rods with diameter d, and Λ is the pitch. (b) SEM image of one of the fabricated LPFs. (c) Calculated intensity profiles of the fundamental LP_{01} and two higher-order modes with the largest overlap with the core region at 1064 nm.

adjacent cladding elements. The germanium-doped inclusions remove mirror symmetries existent in a conventional hexagonal cladding LPF.

A fiber preform was fabricated using the stack-and-draw technique. The germanium-doped rods were drawn from a conventional telecommunications graded index fiber (GIF) preform. The stack was then drawn to fibers of 1000 (LPF-A) and 810 μm (LPF-B) outer diameters (ODs) and 1.15 m in length.

The measured normalized hole-diameters (D/Λ) were 0.395 and 0.355 for LPF-A and LPF-B, respectively. Although, in this case, the fabricated fibers are passive, our fibers are composed of an air clad so that avoided crossings between core and cladding modes are taken into account [30].

Table 1. Parameters of the Fabricated Rod-Type LPFs

	Core Diameter [μm]	Hole Diameter (D) [μm]	Germanium Diameter (d) [μm]	Pitch (Λ)	Air Clad Diameter [μm]	OD [μm]
LPF-A	63	15	6	38	260	1000
LPF-B	53	11	4	31	205	810

Figure 1(b) illustrates a scanning electron microscope (SEM) image of the fabricated LPF-A. Numerical simulations demonstrating a highly confined fundamental mode in the core of the fiber (LPF-A) at the wavelength of 1064 nm, as well as the first two HOMs with the highest overlap with the core region, are depicted in Fig. 1(c). The geometrical parameters of the fabricated reduced symmetry LPFs are summarized in Table 1.

In order to study the modal properties of the fabricated LPFs, a 53/125 μm core/cladding diameter GIF was used to butt-couple white light from a supercontinuum source to the fiber under test. The output beam profiles were then recorded using a microscope objective (with 20× magnification) and an infrared camera. Figure 2 shows the recorded near-field output profiles after propagation along 1.15 m of LPF-A using a 10 nm bandpass filter centered at 1064 nm. For centered excitation, only the fundamental LP_{01}-like mode was observed at 1064 nm as can be seen from Fig. 2. This is despite the fact that the excitation light was multimode and not mode matched to the fundamental mode of the fiber under test. Moreover, the beam quality factor M^2 at the wavelength 1064 nm was measured to be 1.3.

To verify the robust single-mode operation of the fibers under various launching conditions, we misaligned the input beam by translating the GIF along the transverse direction from −30 to +30 μm through 10 μm increments, attempting to excite HOMs. According to the measured output intensity profiles shown in Fig. 2, no HOMs were excited even under rather strong misalignment conditions. Visualization 1 shows the evolution of the near-field intensity profile of the output beam at 1064 nm under transversal displacement of the launch fiber. As it is clear, single-mode behavior with strong delocalization of HOMs is observed. Here we also note that similar output profiles were obtained by scanning a small core single-mode fiber across the entrance facet using a 1064 nm laser source. Moreover, it should be mentioned that LPF-B showed similar performance as fiber LPF-A under various launching conditions. These results confirm the effective single-mode operation and strong HOM delocalization of our reduced symmetry LMA fibers.

In order to study the guidance characteristics of LPF-A and LPF-B as a function of wavelength, near-field intensity profiles were recorded for centered excitation using 10 nm bandpass filters, as depicted in Fig. 3. Both LPF-A and LPF-B exhibit dominant single-mode operation over a broad spectral range of 850–1650 nm with the exception of particular wavelength regions where the core mode couples to the germanium-doped rods. The particular resonant wavelengths, for which the fibers do not provide efficient guidance, depend exclusively on the parameters of the graded index resonators. As can be seen in

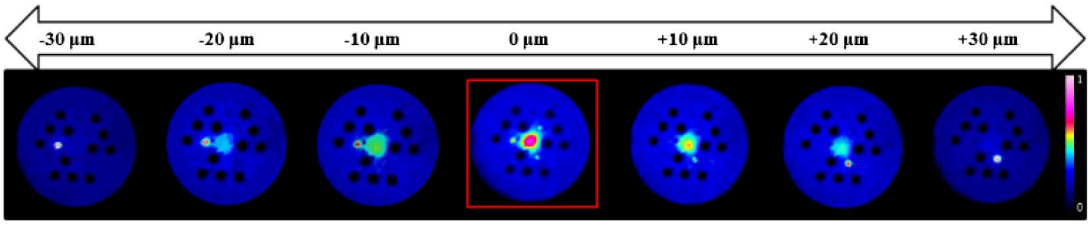

Fig. 2. Near-field intensity profiles measured at 1064 nm at the output of a 1.15 m long LPF-A (Visualization 1). A supercontinuum source was coupled under various launching conditions ranging from −30 to +30 μm attempting to excite any possible HOMs.

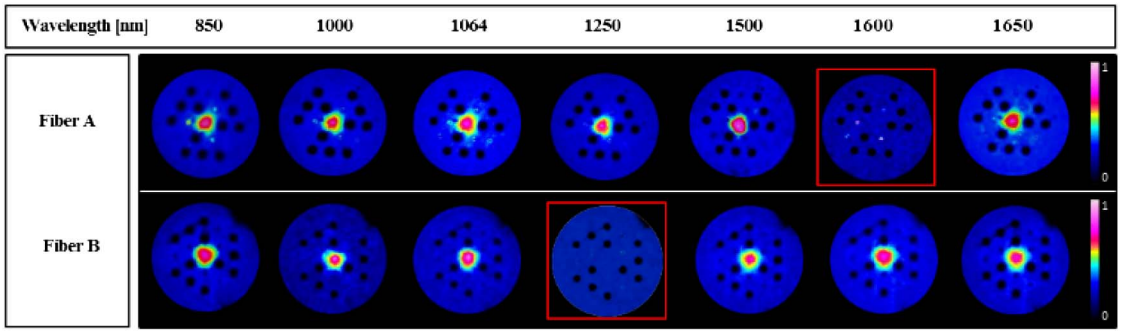

Fig. 3. Near-field mode profiles of the asymmetric rod-type LPF-A and LPF-B over a broad spectral range of 850 to 1650 nm.

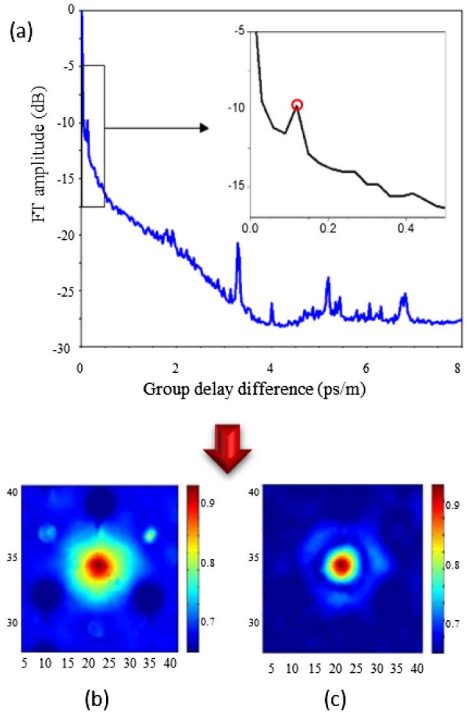

Fig. 4. S^2 measurement of the LPF-A at 1064 nm. (a) FT amplitude of the transmitted light versus GDD, (b) FM profile corresponding to the FT amplitude at GDD = 0 ps/m, and (c) LP_{02}-like profile as the sole HOM detected (corresponding to the peak in GDD indicated by the red circle in the closeup of the FT spectrum in [a]).

Fig. 3, this region is around 1600 nm for LPF-A and 1250 nm for LPF-B.

To further validate the highly effective HOM delocalization and single-mode behavior of the fibers, S^2 resolved imaging was applied [31]. The technique is based on a spatially resolved measurement of the spectral interference between modes propagating simultaneously in the fiber with different group velocities. Figure 4 shows the results of the S^2 measurements for LPF-A at 1064 nm. The Fourier transform (FT) signal at a group delay difference (GDD) of 0 pm/s corresponds to the autocorrelation signal of the fundamental mode guided in the core of the fiber. Therefore, plotting this signal as a function of (x, y) position yields the fundamental mode intensity distribution shown in Fig. 4(b). Due to the spatial distribution of its intensity, the second peak detected at GDD = 0.1193 ps/m, marked as a red circle in the inset of Fig. 4(a), is attributed to a small content of a radially symmetric LP_{02}-like mode. From the amplitude of the FT, the amount of LP_{02}-like modes excited in the fiber can be quantified to be 0.28%. Other features in the FT spectrum with even smaller FT amplitudes do not correspond to any particular HOM guided in the asymmetric LPF; hence, they are attributed to the small amounts of excited cladding modes supported by the fiber.

Our results indicate that in similar active fibers based on the proposed asymmetric LPF designs, LP_{11}-like HOMs, which are the most disturbing modes in detrimental MI effects in high-power fiber amplifiers, can perhaps be very strongly suppressed compared to conventional symmetric LMA fiber designs. Such strong HOM suppression confirms the potential of the investigated asymmetric LMA fiber to significantly increase MI thresholds and enable higher output powers of fiber lasers and amplifiers before the onset of beam quality distortions.

In conclusion, we designed, fabricated, and characterized a reduced symmetry passive LMA rod-type fiber with near-diffraction-limited beam quality of $M^2 = 1.3$ and effective mode area of 2560 μm^2 at 1064 nm. The fabricated fibers included six high-index germanium-doped silica elements inserted asymmetrically in the cladding lattice in order to suppress LP_{11}-like HOMs guiding in the fiber core. No significant HOM content was observed, even for strongly misaligned coupling of light relative to the fiber core center.

The effective HOM delocalization of the fiber has been shown across a broad spectral range from 850 to 1650 nm for different core diameters. Further investigations using S^2 imaging showed a negligible amount of LP_{02} (0.28%) in the fiber, confirming the robustness of single-mode operation and the strong suppression of LP_{11}-like modes. This LPF design with an asymmetric cladding structure is a promising route to improve the threshold-like onset of MI in high-power fiber lasers and amplifiers.

Funding. Air Force Office of Scientific Research (AFOSR) (FA9550-15-10041); Army Research Office (ARO) (W911NF-12-1-0450); High Energy Laser Joint Technology Office (HEL JTO) (W911NF-12-1-0450).

REFERENCES

1. J. Limpert, N. Deguil-Robin, I. Manek-Honninger, F. Salin, F. Roser, A. Liem, T. Schreiber, S. Nolte, H. Zellmer, A. Tunnermann, J. Broeng, A. Petersson, and C. Jakobsen, Opt. Express **13**, 1055 (2005).

2. D. J. Richardson, J. Nilsson, and W. A. Clarkson, J. Opt. Soc. Am. B **27**, B63 (2010).
3. J. Nilsson and D. N. Payne, Science **332**, 921 (2011).
4. C. Jauregui, J. Limpert, and A. Tünnermann, Nat. Photonics **7**, 861 (2013).
5. M. N. Zervas and C. A. Codemard, IEEE J. Sel. Top. Quantum Electron. **20**, 219 (2014).
6. J. Limpert, A. Liem, M. Reich, T. Schreiber, S. Nolte, H. Zellmer, A. Tünnermann, J. Broeng, A. Petersson, and C. Jakobsen, Opt. Express **12**, 1313 (2004).
7. J. Limpert, O. Schmidt, J. Rothhardt, F. Röser, T. Schreiber, A. Tünnermann, S. Ermeneux, P. Yvernault, and F. Salin, Opt. Express **14**, 2715 (2006).
8. E. M. Dianov, M. E. Likhachev, and S. Fevrier, IEEE J. Sel. Top. Quantum Electron. **15**, 20 (2009).
9. F. Jansen, F. Stutzki, H.-J. Otto, T. Eidam, A. Liem, C. Jauregui, J. Limpert, and A. Tünnermann, Opt. Express **20**, 3997 (2012).
10. F. Stutzki, F. Jansen, T. Eidam, A. Steinmetz, C. Jauregui, J. Limpert, and A. Tünnermann, Opt. Lett. **36**, 689 (2011).
11. J. Limpert, F. Stutzki, F. Jansen, H.-J. Otto, T. Eidam, C. Jauregui, and A. Tünnermann, Light Sci. Appl. **1**, e8 (2012).
12. T. T. Alkeskjold, M. Laurila, L. Scolari, and J. Broeng, Opt. Express **19**, 7398 (2011).
13. H.-J. Otto, F. Stutzki, N. Modsching, C. Jauregui, J. Limpert, and A. Tünnermann, Opt. Lett. **39**, 6446 (2014).
14. W. S. Wong, X. Peng, J. M. McLaughlin, and L. Dong, Opt. Lett. **30**, 2855 (2005).
15. L. Dong, X. Peng, and J. Li, J. Opt. Soc. Am. B **24**, 1689 (2007).
16. C.-H. Liu, G. Chang, N. Litchinister, D. Guertin, N. Jacobson, K. Tankala, and A. Galvanauskas, in *Conference on Lasers and Electro-Optics/Quantum Electronics and Laser Science Conference and Photonic Applications Systems Technologies* (Optical Society of America, 2007), p. CTuBB3.
17. X. Ma, C. Zhu, I.-N. Hu, A. Kaplan, and A. Galvanauskas, Opt. Express **22**, 9206 (2014).
18. M. Laurila, J. Saby, T. T. Alkeskjold, L. Scolari, B. Cocquelin, F. Salin, J. Broeng, and J. Lægsgaard, Opt. Express **19**, 10824 (2011).
19. M. Laurila, M. M. Jørgensen, K. R. Hansen, T. T. Alkeskjold, J. Broeng, and J. Lægsgaard, Opt. Express **20**, 5742 (2012).
20. T. Eidam, C. Wirth, C. Jauregui, F. Stutzki, F. Jansen, H.-J. Otto, O. Schmidt, T. Schreiber, J. Limpert, and A. Tünnermann, Opt. Express **19**, 13218 (2011).
21. C. Jauregui, T. Eidam, H.-J. Otto, F. Stutzki, F. Jansen, J. Limpert, and A. Tünnermann, Opt. Express **20**, 12912 (2012).
22. C. Jauregui, T. Eidam, H.-J. Otto, F. Stutzki, F. Jansen, J. Limpert, and A. Tünnermann, Opt. Express **20**, 440 (2012).
23. A. V. Smith and J. J. Smith, Opt. Express **19**, 10180 (2011).
24. B. Ward, C. Robin, and I. Dajani, Opt. Express **20**, 11407 (2012).
25. K. R. Hansen, T. T. Alkeskjold, J. Broeng, and J. Lægsgaard, Opt. Express **21**, 1944 (2013).
26. F. Stutzki, F. Jansen, H.-J. Otto, C. Jauregui, J. Limpert, and A. Tünnermann, Optica **1**, 233 (2014).
27. F. Stutzki, F. Jansen, C. Jauregui, J. Limpert, and A. Tünnermann, Opt. Express **19**, 12081 (2011).
28. R. Dauliat, D. Gaponov, A. Benoit, F. Salin, K. Schuster, R. Jamier, and P. Roy, Opt. Express **21**, 18927 (2013).
29. A. Benoît, R. Dauliat, R. Jamier, G. Humbert, S. Grimm, K. Schuster, F. Salin, and P. Roy, Opt. Lett. **39**, 4561 (2014).
30. F. Jansen, F. Stutzki, C. Jauregui, J. Limpert, and A. Tünnermann, Opt. Express **19**, 13578 (2011).
31. J. W. Nicholson, A. D. Yablon, S. Ramachandran, and S. Ghalmi, Opt. Express **16**, 7233 (2008).